Materials Today Communications 35 (2023) 106048

Contents lists available at ScienceDirect

Materials Today Communications

journal homepage: www.elsevier.com/locate/mtcomm

Efficient electrocatalytic properties of transition metal (Mn, Co, Cu) doped $LaFeO_3$ for ammonia synthesis via nitrate reduction

Qi Yin, Hao Zhou *

State Key Laboratory of Clean Energy Utilization, Zhejiang University, Hangzhou 310027, China

ARTICLE INFO

Keywords:
Nitrate reduction
Ammonia synthesis
Perovskite
Oxygen vacancy

ABSTRACT

Electrochemical reduction of nitrate in wastewater to synthesize high-value energy, ammonia, is a promising technology to deal with the energy crisis and environmental pollution. It is an urgent task for this technology to find efficient, stable and environmental-friendly catalysts. This work innovatively applied transition metal (Mn, Co, Cu) doped $LaFeO_3$ as the electrocatalyst to reduce nitrate to ammonia. Cu-doped $LaFeO_3$ exhibited the optimum activity, achieving the ammonia yield of 1005.0 μg $h^{-1}cm^{-2}$ at − 1.1 V (vs. RHE) and the Faradaic efficiency of 71.9% at − 1.0 V (vs. RHE). The highly efficient electrocatalytic activity could be mainly attributed to the oxygen vacancies on the surface of the catalyst generated from Cu-doping. The oxygen atoms in the nitrate tended to fill in the oxygen vacancies, which promoted the adsorption of NO_3 and weakened the N-O bonds. Besides, the oxygen vacancies and Cu sites could combine easily with the intermediate in the reaction, and their existence could also enhance the conductivity of the catalyst. Moreover, the catalyst showed outstanding stability and performed even enhanced activity during recycling, which was arised from the ferroelectricity of the catalyst. The ammonia yield was as high as 1250.5 μg $h^{-1}cm^{-2}$ in the third cycle, and the Faradaic efficiency was 74.5% in the fifth cycle at − 1.0 V (vs. RHE). This work presents a good paradigm of catalysts for the electrochemical synthesis of ammonia.

1. Introduction

Ammonia (NH_3) is a promising energy carrier because it is carbon-free, hydrogen-rich and has a high energy density. Besides, it is irreplaceable in the chemical industry, agriculture and medicine. Currently, the Haber-Bosch process is mainly employed in industry to synthesize ammonia, while high temperature (300–500 ℃) and high pressure (200–300 bar) are necessary conditions, which can lead to high energy consumption and carbon dioxide emissions [1–4]. With the development of renewable energy such as solar energy and wind energy, electrochemical synthesis of ammonia is becoming a competitive method. However, nitrogen (N_2) has little potential to be used as a raw material for industrial electrochemical synthesis of ammonia due to the high dissociation energy (941 kJ mol^{-1} for N≡N), low proton affinity and low solubility [5,6]. As a widely existing pollutant in water, nitrate (NO_3^-) is gradually regarded as an alternative raw material for the electrochemical synthesis of ammonia for the low dissociation energy of the N = O bond (204 kJ mol^{-1}) [5]. Therefore, it has attracted extensive attention worldwide to reduce nitrate in wastewater to ammonia through an electrochemical route. This technology is expected to play a remarkable role in response to the energy crisis and environmental pollution, which makes it the most pressing demand of the day to find efficient and stable catalytic electrode materials.

Among metal-based catalysts, some transition metal (TM) elements like Cu [5–8], Co [9,10], and Ni [11,12] have been proved to have the ability of electrocatalytic reduction of nitrate. It is well known that Fe in nitrogenase plays a vital role in the natural nitrogen fixation system. The key role of Fe in the catalysts of Haber-Bosch process also proves that Fe can serve as important active sites for ammonia synthesis. And Fe has moderate binding ability with oxygen and nitrogen, and is expected to exhibit good activity of reducing nitrate. Moreover, Fe is one of the most abundant elements in the Earth's crust, far surpassing other transition metal elements, with low prices and environmental friendliness. Previous work has demonstrated the remarkable ability of Fe-based materials to electrochemically reduce nitrate to ammonia [13–15]. Wu et al. [13] reported a selective and active nitrate reduction to ammonia on Fe single atom catalyst, with a maximal ammonia Faradaic efficiency of ~ 75% and a yield rate of up to 0.46 mmol h^{-1} cm^{-2}. Wang et al. [14] prepared

* Corresponding author.
E-mail address: zhouhao@zju.edu.cn (H. Zhou).

https://doi.org/10.1016/j.mtcomm.2023.106048
Received 29 November 2022; Received in revised form 13 April 2023; Accepted 20 April 2023
Available online 23 April 2023

N-doped carbon nanosheets supported Fe_3C nanoflakes, and the NH_3 yield and faradaic efficiency were up to 1.19 mmol h^{-1} mg^{-1} and 96.7%, respectively. Liu et al. [15] reported that FeOOH nanorod reduced nitrate to ammonia with the yield of 2419 μg h^{-1} cm^{-2} and the Faradic efficiency of 92%. Although only a few studies have investigated the ability of perovskites as electrocatalysts of NO_3^- reduction reaction (NO_3RR) until now, Fe-based perovskites were still selected in the first place among perovskite materials. In 2022, Wang et al. [16] reported that $BiFeO_3$ flakes with a distorted perovskite-type structure could deliver an excellent performance for electrochemical NO_3RR. Also in 2022, Yang et al. [17] compared the electrocatalytic abilities of four perovskite oxide cathodes, $LaMO_{3-\delta}$ (M = Fe, Co, Ni and Cu) for NO_3RR. According to their work, the Ruddlesden-Popper type La_2CuO_4 performed a better electrocatalytic activity than Fe-based perovskite, $LaFeO_3$. In 2023, Zheng et al. [18] reported that $LaCoO_3$ surpassed $LaFeO_3$ and other three perovskite as the electrocatalyst for NO_3RR. In the above studies, the potential of Fe-based perovskites for electrochemical NO_3RR has not been fully explored, and specific methods to improve the ability of Fe-based perovskites need to be proposed. Besides, ferroelectricity is an important property of many perovskite materials, and its influence on electrochemical NO_3RR was not discussed in the above studies.

Herein, we synthesized perovskite $LaFeO_3$ by a sol-gel method employed it as the catalyst for electrochemical synthesis of NH_3 from NO_3^-. In order to furthur exploit the catalytic potential of $LaFeO_3$, oxygen vacancy engineering is a feasible idea [19–23]. We selected several typical transition metals (Mn, Co, Cu) to modify $LaFeO_3$ by B-site doping, as transition metal atom doping is often employed to form a large number of oxygen vacancies on the surface of perovskite. The doped $LaFeO_3$ catalysts were also employed for electrochemical NH_3 synthesis to compare their activities with the original $LaFeO_3$ catalyst. The results showed that Co or Cu doping was conducive to the electrocatalytic activity of the catalysts, and Cu-doped $LaFeO_3$ exhibited the optimum electrocatalytic ability. Moreover, Cu-doped $LaFeO_3$ not only performed excellent stability, but also showed an upward trend as to the ammonia yield and the Faradaic efficiency in consecutive recycling experiments, which was arised from the ferroelectricity of the catalyst. Finally, we proposed the mechanism of the highly efficient electrochemical reduction of nitrate to ammonia on Cu-doped $LaFeO_3$ after discussion. The highly efficient electrocatalytic activity was mainly attributed to the existence of oxygen vacancies due to Cu-doping.

2. Experimental

2.1. Preparation of catalysts

The original $LaFeO_3$ and TM doped samples, $LaFe_{0.9}TM_{0.1}O_{3-\delta}$ (TM=Mn, Co, Cu), were synthesized by a standard sol-gel method [24, 25]. In a typical procedure, lanthanum nitrate hexahydrate ($La(NO_3)_3$`6 $H_2O$, 99.9%) and iron nitrate nonahydrate ($Fe(NO_3)_3$`9 H_2O, 98.5%) were dissolved with deionized water according to the stoichiometric ratio. Ethylenediamine tetraacetic acid (EDTA, AR) and citric acid monohydrate (CA, 99.5%) were then added following the molar ratio of total metal ions: EDTA: CA= 1: 1: 2.5. The pH of the solution was adjusted to ~6 with the ammonia solution (25.0–28.0%). After that, the solution was stirred in a water bath at 90 ℃ for ~2 h to obtain a transparent gel. The gel was dried in the air at 200 ℃ for 2.5 h to obtain a solid precursor. And then, it was calcined at 650 ℃ for 3 h in the air to obtain the original $LaFeO_3$ sample (denoted as LF). The TM doped samples, $LaFe_{0.9}TM_{0.1}O_{3-\delta}$ (TM=Mn, Co, Cu) (denoted as LFMn, LFCo, LFCu, respectively) were synthesized via a similar procedure, with the dosage of $Fe(NO_3)_3$`9 $H_2O$ reduced and the addition of manganese nitrate hexahydrate ($Mn(NO_3)_2$`6 H_2O, 98%), cobalt nitrate hexahydrate ($Co(NO_3)_2$`6 $H_2O$, 99%), or copper nitrate hydrate ($Cu(NO_3)_2$`x H_2O, 99.99%) according to the stoichiometric ratio.

2.2. Characterization

X-ray diffraction (XRD) patterns of prepared samples were recorded by BrukerAXS D8 (Cu Kα radiation, scan rate = 5°/min) to determine the composition of the samples. The microscopic morphologies of the samples were photographed by scanning electron microscope (SEM, ZEISS Gemini 300, acceleration voltage = 3.0 kV). An energy dispersive spectrometer (EDS, Oxford Xplore, acceleration voltage = 15.0 kV) equipped on the SEM was employed to determine the elemental composition of the samples. Inductively coupled plasma-optical emission spectroscopy (ICP-OES, Agilent 720ES) was employed to determine the chemical composition of prepared catalysts. X-ray photoelectron spectroscopy (XPS) patterns of the samples were recorded by Thermo Scientific K-Alpha (Al Ka radiation, hν=1486.6 eV) to investigate the composition and valence states of the elements.

2.3. Electrochemical ammonia synthesis

The working electrode used in the electrochemical reaction was formed by clamping carbon paper (CP) with a platinum electrode clamp. The CP had an exposed area of 1 × 1 cm^2 and had been coated with the catalyst several times to form a covering of 1 mg/cm^2. The ink used for coating the catalyst was a homogeneous suspension formed by sonication of 5 mg catalyst and 40 μL Nafion solution (5 wt%) in 960 μL ethanol solution (V_{water}: $V_{ethanol}$ = 1: 3).

Electrochemical experiments were performed using an electrochemical workstation (CHI 660E, CH Instruments, Shanghai) to control a standard H-type three-electrode reaction system. The two cells were separated by a Nafion117 membrane treated at 80 ℃ with 5 wt% hydrogen peroxide for 1 h, deionized water for 0.5 h, 5 wt% dilute sulfuric acid for 1 h and deionized water for 0.5 h beforehand. Besides the working electrode mentioned above, the reference electrode was an Ag/AgCl electrode (saturated with KCl), and the counter electrode was a Pt foil electrode. The anode electrolyte was 45 mL 0.1 M Na_2SO_4 solution, and the cathode electrolyte was 45 mL 0.1 M Na_2SO_4/0.1 M $NaNO_3$ (unless otherwise stated in the control experiments). Before each test, Ar was bubbled into the cathode electrolyte with magnetic stirring for 30 min. And then, a Cyclic Voltammetry (CV) process was performed (100 mV s^{-1}) to activate the catalyst and stabilize the reaction system. In Linear Sweep Voltammetry (LSV) tests, the scanning rate was settled at 5 mV s^{-1}. Amperometric i-t curves were employed to perform electrochemical reactions for 2 h. Ar bubbling and magnetic stirring were kept all the time.

2.4. Determination of products

After 2 h of electrochemical reaction, the cathode electrolyte was taken to determine the products. The concentration of ammonia was determined by the indophenol blue method (see the Supplementary Information for details) [26,27]. The concentration of by-product, nitrite (NO_2^-), was detected referring to previous work (see the Supplementary Information for details) [12].

The yield (μg $h^{-1}cm^{-2}$) of product X (X = NH_3 or NO_2^-) was calculated as:

$$Y_X = \frac{c_X \times V}{t \times A}$$

where c_X (μg mL^{-1}), V (mL), t (h), and A (cm^2) were the concentration of X, the volume of cathode electrolyte, the reaction time and the geometric area of the working electrode, respectively.

The Faradaic efficiency for NH_3 production was calculated as:

$$FE_{NH_3} = \frac{8F \times c_{NH_3} \times V \times 10^{-6}}{M_{NH_3} \times Q}$$

where M_{NH_3} (g mol^{-1}) and Q (C) were the molar mass of NH_3 and the

total charge passing through the electrode, respectively. And F referred to the Faraday constant (96485 C mol^{-1}).

$[NO_2^-]/[NH_3]$ was defined as the molar ratio of NO_2^- and NH_3 in the products to evaluate the selectivity of the reaction, and it was calculated as:

$$[NO_2^-]/[NH_3] = \frac{c_{NO_2^-}/M_{NO_2^-}}{c_{NH_3}/M_{NH_3}}$$

where $M_{NO_2^-}$ (g mol^{-1}) was the molar mass of NO_2^-.

3. Results and discussion

3.1. Characterization of as-prepared catalysts

Fig. 1(a) shows the overall XRD patterns of LF, LFMn, LFCo, and LFCu samples. The patterns are all consistent with PDF#88–0641. All three doped samples had a pure orthorhombic crystal structure (space group Pnma) as the original LF sample. Transition metal doping does not lead to impurity peaks. Fig. 1(b) presents the partially enlarged XRD patterns of the prepared samples. The figure shows that the main peak corresponding to the (1 2 1) plane shifted slightly to a higher angle after doping the transition metal, which was consistent with previous studies [28–30]. This indicated that transition metal ions were successfully doped into the lattice of perovskite. The difference between the radius of transition metal ions and Fe^{3+} ions causes the inclination of FeO_6 octahedra, which leads to the shift of peak position.

The microscopic morphologies of the samples were photographed by SEM, as shown in Fig. 2. It could be estimated that the particle size of the LF catalyst was about 50 nm according to Fig. 2(a). The particle size of LFCo was similar to LF (Fig. 2(c)), while that of LFCu was smaller (Fig. 2 (d)). The particle size of LFMn was the smallest among all catalysts, which was estimated to be only 20–30 nm according to Fig. 2(b). Fig. 3 displays the EDS mappings of transition metal doped samples. It is apparent in the figures that La, Fe, O and transition metal elements were evenly distributed in the doped samples. This confirmed the conclusion of XRD tests that transition metals were successfully doped into the lattice of perovskite. Table 1 shows the weight percentage of La, Fe, and the doped TM elements in the prepared catalysts. Accordingly, the molar ratios of La, Fe and doped TM elements in the catalysts were calculated as 1: 0.94: 0.11, 1: 0.92: 0.10, and 1: 0.90: 0.08 for LFMn, LFCo, and LFCu respectively. This indicated that $LaFe_{0.9}TM_{0.1}O_{3-\delta}$ (TM=Mn, Co, Cu) were successfully synthesized by the sol-gel method stated in this paper.

XPS spectra of prepared samples were recorded to investigate the composition and valence states of the elements, as shown in Fig. 4. Fig. 4 (a) shows the Mn 2p spectrum of LFMn. It could be concluded that Mn 2p peaks had significantly split spin-orbit components, and the spin-orbit gap difference between Mn $2p_{3/2}$ and Mn $2p_{1/2}$ was about 11.6 eV. The peaks located at 641.7 and 644.0 eV corresponded to the 3 + and 4 + oxidation states of Mn, respectively [28]. Besides, a dwarf satellite peak was also observed, indicating that there may be a small amount of Mn in the 2 + oxidation state. Fig. 4(b) displays the Co 2p spectrum of LFCo. The Co^{3+} 2p peak was split into a group of double peaks located at 779.9 and 794.6 eV, respectively, due to spin-orbit splitting, and the spin-orbit gap difference was about 14.7 eV. Similarly, a set of double peaks located at 782.4 and 797.4 eV were assigned to Co^{2+} $2p_{3/2}$ and Co^{2+} $2p_{1/2}$, respectively. In addition, several satellite peaks were also observed on the spectrum. The above characteristics indicated that Co existed in the mixed oxidation state of Co^{2+}/Co^{3+} [31–33]. The Cu 2p spectrum of LFCu is shown in Fig. 4(c). A group of double peaks located at 933.1 and 952.8 eV with a spin-orbit gap difference of 19.7 eV were observed, as well as two satellite peaks with strong signals. This proved the existence of + 2 oxidation state of Cu in the LFCu catalyst. Besides, the peaks located at 932.7 and 952.2 eV were assigned to Cu^+ $2p_{3/2}$ and Cu^+ $2p_{1/2}$, respectively. The characteristics of the spectrum illustrated the mixed oxidation state of Cu^+/Cu^{2+} in the LFCu catalyst [17,30].

Fig. 4(d) displays the O 1 s spectra of LF, LFMn, LFCo, and LFCu. There are four peaks located at 528.8–529.3, 530.4, 531.3 and 532.7 eV, respectively, corresponding to lattice oxygen ($O_{lattice}$), highly oxidative oxygen species (O_2^{2-}/O^-), surface adsorbed oxygen or hydroxyl groups (O_{ads}), and surface-adsorbed water (O_{H2O}), respectively [25,34,35]. The figure clearly shows that the order of O_2^{2-}/O^- content in each catalyst from high to low was LFCu > LFCo > LF > LFMn. The atomic percentage of different kinds of oxygen species measured from the O 1 s spectra was shown in Table 2, which confirms the information in the figure. The atomic percentage of O_2^{2-}/O^- in all oxygen elements in the original LF catalyst was 2.85%. In LFCo and LFCu, this value increased to 5.71% and 8.34%, respectively, which was 2.0 and 2.9 times that of the original LF catalyst. However, the content of O_2^{2-}/O^- in LFMn was less than that in LF, only 1.5%. Previous studies have stated that O_2^{2-}/O^- species were closely related to the surface oxygen vacancies of catalysts [25,34]. The increase of O_2^{2-}/O^- content in LFCo and LFCu indicated that a large number of oxygen vacancies were generated on the surface under the influence of charge balance after Co or Cu was doped in the perovskite lattice. Cu doping was more beneficial because Cu existed in the oxidation state of Cu^+/Cu^{2+}, while Co existed as Co^{2+}/Co^{3+}, and the former had a greater charge difference with the replaced Fe^{3+}. However, Mn mainly existed in the oxidation state of + 3 and less in the oxidation state of + 4, so few oxygen vacancies formed on the surface of LFMn.

3.2. Electrochemical experiments

LSV tests were conducted to assess whether the prepared catalysts

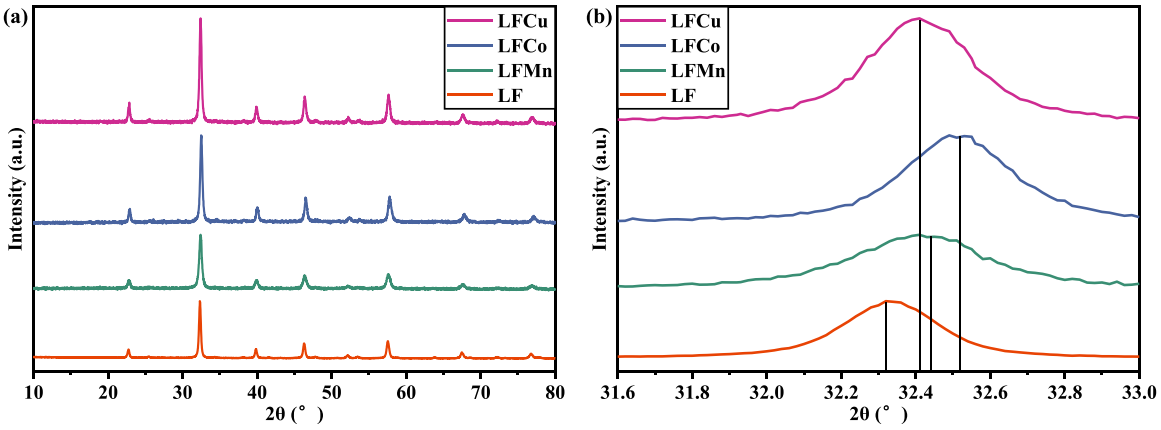

Fig. 1. (a) Overall and (b) partial XRD patterns of as-prepared LF, LFMn, LFCo, and LFCu.

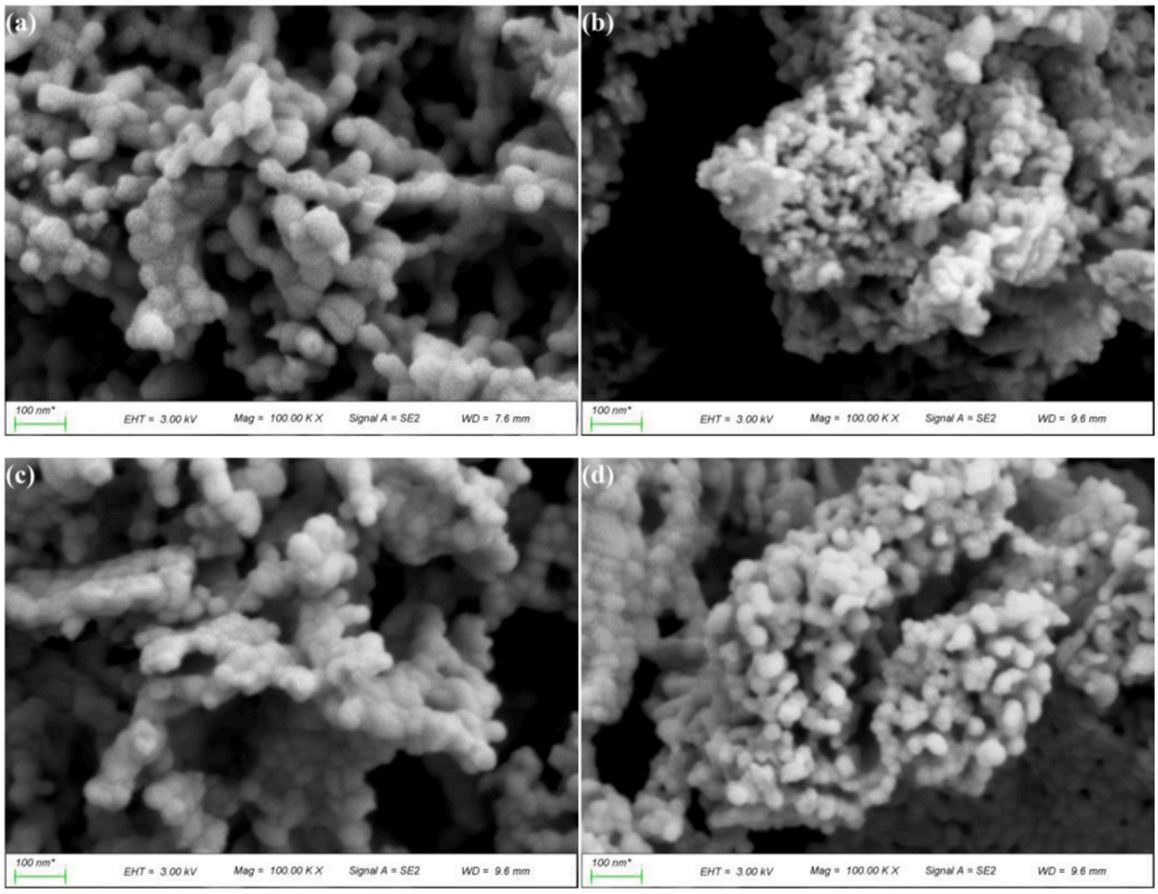

Fig. 2. SEM images of (a) LF, (b) LFMn, (c) LFCo, and (d)LFCu.

could reduce nitrate to ammonia, as shown in Fig. 5(a). Potentials throughout this work were remarked referring to reversible hydrogen electrode (RHE) according to the Nernst equation [12]:

$$E_{RHE} = E_{Ag/AgCl} + 0.059 \times pH + 0.198$$

LSV curves showed that in the tested potential range, when the electrolyte contained nitrate, the current density flowing through the LF electrode was larger than that when the electrolyte contained no nitrate. The difference of the current density proved that the original LF catalyst had the ability to reduce nitrate. For a TM doped catalyst (taking LFCu as an example), the current density flowing through the electrode was larger than that of the LF electrode, especially when there was nitrate in the electrolyte. This illustrated that TM doping was expected to improve the electrocatalytic ability of LF perovskite, especially the ability of nitrate reduction.

Experimental results of electrochemical nitrate reduction using different catalysts are presented in Fig. 5(b). The original LF could achieve the NH_3 yield of 49.0 μg $h^{-1}cm^{-2}$ and the Faradaic efficiency of 50.7% at − 0.7 V. After doping Co or Cu, the activity of the catalysts was significantly improved. The NH_3 yield of LFCo and LFCu was 72.6 and 104.0 μg $h^{-1}cm^{-2}$, respectively, which was 1.5 and 2.1 times that of original LF, respectively. The Faradaic efficiency of LFCo and LFCu was 50.9% and 51.5%, respectively, which was also higher than that of the original LF. However, LFMn could only achieve the NH_3 yield of 46.2 μg $h^{-1}cm^{-2}$ and the Faradaic efficiency of 44.0%, and the catalytic activity was worse than that of the original LF. The catalytic activity of all prepared catalysts was LFCu > LFCo > LF > LFMn from high to low. This was consistent with the order of the content of oxygen vacancies on the catalysts. It confirmed the conclusions of previous studies that oxygen vacancies on the surface of catalysts had a significant positive effect on the activity of nitrate reduction [19–23].

Experiments of electrochemical reduction of nitrate at different potentials using LFCu were conducted to find the optimum potential, as shown in Fig. 6(a). As the potential varied from − 0.6 V to − 1.1 V, the NH_3 yield increased significantly from 53.3 μg $h^{-1}cm^{-2}$ at − 0.6 V to 1005.0 μg $h^{-1}cm^{-2}$ at − 1.1 V, and the latter was nearly 19 times that of the former. When the potential changed from − 0.6 V to − 1.0 V, the Faradaic efficiency increased continuously, reaching the maximum (71.9%) at − 1.0 V. However, when the potential became more negative (−1.1 V), the Faradaic efficiency slightly decreased to 70.6%. This slight decrease was due to the competitive hydrogen evolution reaction (HER) at more negative potentials. This was consistent with Fig. 5(a). Even if no nitrate was added to the electrolyte, the current density became larger when the potential became more negative, which indicated that HER occurred.

Fig. 6(b) displays the production of another product, NO_2^-, of the electrochemical reduction of nitrate using the LFCu catalyst. As the negative potential changed from − 0.6 V to − 1.1 V, NO_2^- yield presented an overall upward trend. In order to clearly present whether the product was primarily nitrite or ammonia, we defined the molar ratio of nitrite to ammonia, $[NO_2^-]/[NH_3]$, as described in Section 2.4. As shown in Fig. 6(b), $[NO_2^-]/[NH_3]$ was 3.15 at the potential of − 0.6 V, indicating that nitrite was the main product at this potential. $[NO_2^-]/[NH_3]$ decreased with the potential getting more negative, and it decreased to 0.50 when the potential was − 0.9 V, demonstrating that the main product changed from NO_2^- to NH_3. $[NO_2^-]/[NH_3]$ further decreased and maintained less than 1 when the potential changed from − 0.9 to − 1.1 V, which proved that NH_3 was dominant in the products within this potential range. Finally, $[NO_2^-]/[NH_3]$ reached the minimum of 0.27 at − 1.1 V. In this case, the selectivity of NH_3 in the products after reaction was remarkable, and the output of the by-product NO_2^- was relatively small. The above discussion demonstrated that the selectivity

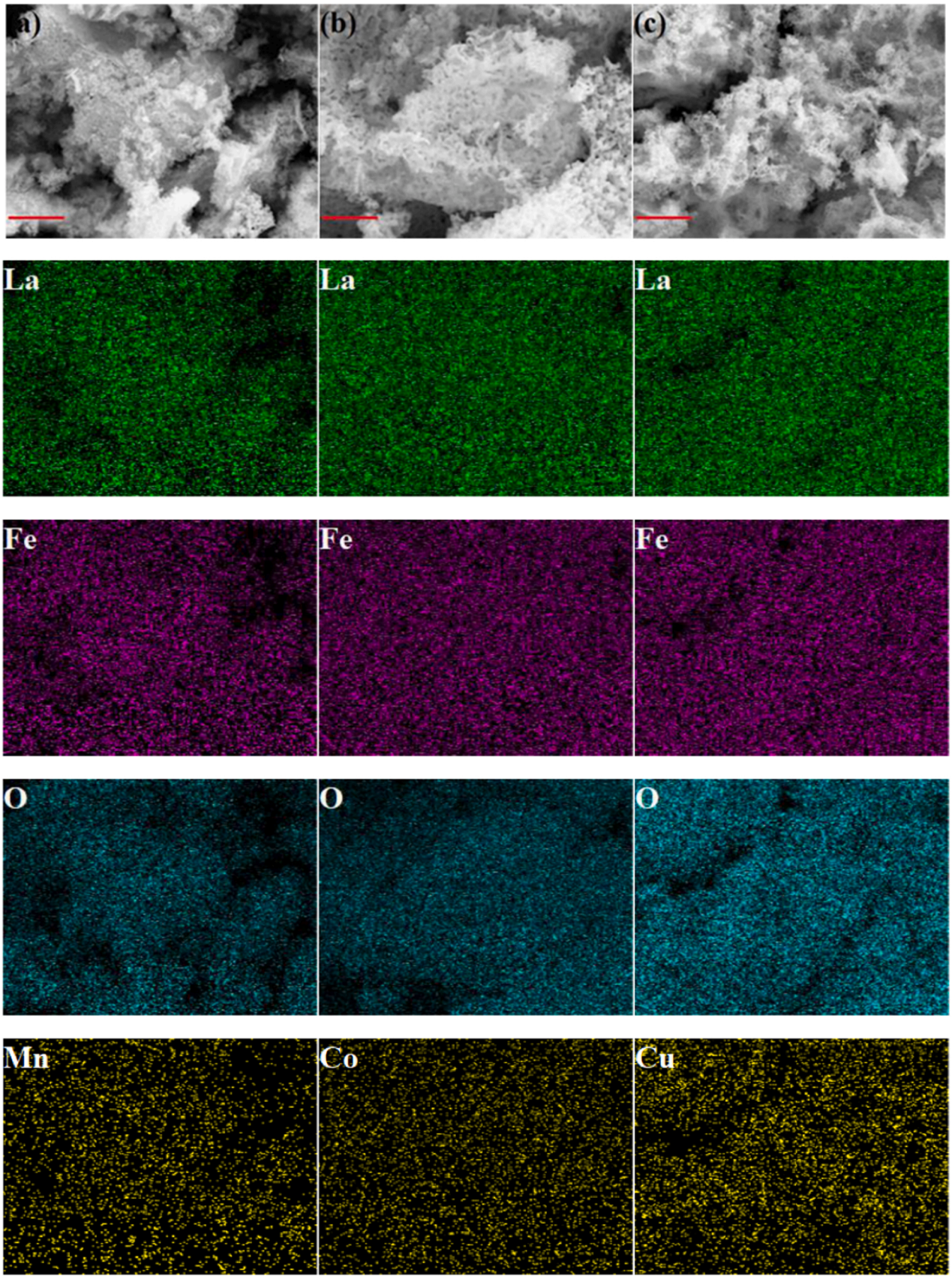

Fig. 3. EDS mappings of (a) LFMn, (b) LFCo, and (c) LFCu (scale bar: 1 μm).

Table 1
Chemical composition of prepared catalysts measured by ICP-MS.

Catalyst	Weight percentage (%)			La: Fe: TM (molar ratio)
	La	Fe	TM	
LFMn	57.66	21.79	2.43	1: 0.94: 0.11
LFCo	57.25	21.21	2.51	1: 0.92: 0.10
LFCu	57.31	20.70	2.04	1: 0.90: 0.08

of the reaction could be optimized to obtain the desired product, NH_3, by choosing the appropriate reaction potential.

Consecutive recycling experiments were conducted at − 1.0 V to test the stability of LFCu catalyst, as shown in Fig. 6(c). The results showed that the NH_3 yield did not decrease but even increased obviously after multiple cycles. The NH_3 yield in the third cycle was even as high as 1250.5 μg $h^{-1}cm^{-2}$, and in the fifth cycle it was 1168.1 μg $h^{-1}cm^{-2}$, which was also higher than 807.9 μg $h^{-1}cm^{-2}$ in the first cycle. After several cycles, the Faradaic efficiency did not decrease but showed a slight upward trend, reaching 74.5% in the fifth cycle, which was higher than 71.9% in the first cycle. The increased electrochemical activity of prepared LFCu catalyst during recycling may arise from the ferroelectricity of lanthanum ferrite material. When the fresh LFCu catalyst underwent the first cycle, ferroelectric polarization occurred under the influence of the applied electric field. As the catalyst was employed in the subsequent cycles, the residual polarization promoted the charge seperation and facilitated the charge transfer between the catalyst and the electrolyte [36–38]. Thus, the electrochemical activity of prepared LFCu catalyst was not weakened but boosted during cyclic experiments. This indicated that LFCu catalyst had excellent cyclic stability and was expected to meet the demand of industrialization.

Control experiments (Fig. 6(d)) were carried out to verify whether NH_3 produced in this work was formed by the electrochemical reduction of NO_3^- on the prepared catalysts. The NH_3 yield was only 14.5 μg $h^{-1}cm^{-2}$ on the bare carbon paper at − 0.7 V, which was far lower than LFCu catalyst (104.0 μg $h^{-1}cm^{-2}$) at the same potential. And almost no NH_3 was detected in the electrolyte without NO_3^- in the electrolyte or at the open circuit potential. These control experiments were sufficient to prove that the NH_3 synthesized in this work was generated by the electroreduction of NO_3^- on the prepared catalysts.

The schematic model of electrocatalytic reduction of NO_3^- to NH_3 on LFCu catalyst was presented, as shown in Fig. 7, according to the characterization tests and the electrochemical experiments. It is well known that the electrochemical reduction of nitrate to ammonia can be divided into two steps [23]. First, NO_3^- is adsorbed and converted to $*NO_2$, which is the rate-determining step. Second, $*NO_2$ was converted to products, which is the selectivity-determining step. When a small amount of Fe^{3+} in the LFCu catalyst was replaced by Cu^+/Cu^{2+}, oxygen vacancies were generated on the surface of the catalyst in order to achieve charge balance. The oxygen atoms in NO_3^- would fill in the

Table 2
Atomic percentage of different kinds of oxygen species measured by XPS.

Catalyst	$O_{lattice}$	O_2^{2-}/O^-	O_{ads}	O_{H2O}
LF	60.73	2.85	31.11	5.32
LFMn	58.94	1.5	31.62	7.95
LFCo	55.23	5.71	30.82	8.25
LFCu	44.92	8.34	39.08	7.66

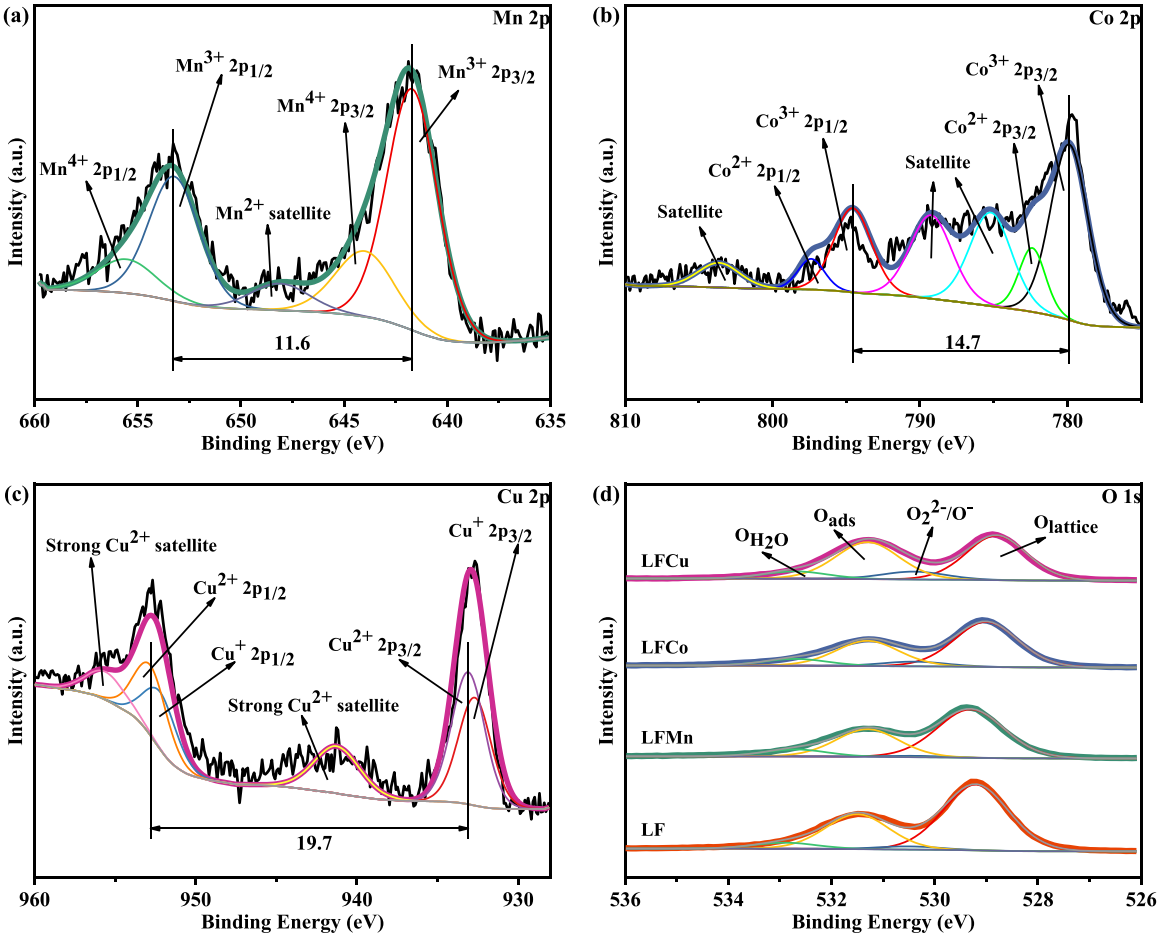

Fig. 4. XPS spectra of (a) Mn 2p of LFMn, (b) Co 2p of LFCo, (c) Cu 2p of LFCu and (d) O 1 s of LF, LFMn, LFCo, and LFCu.

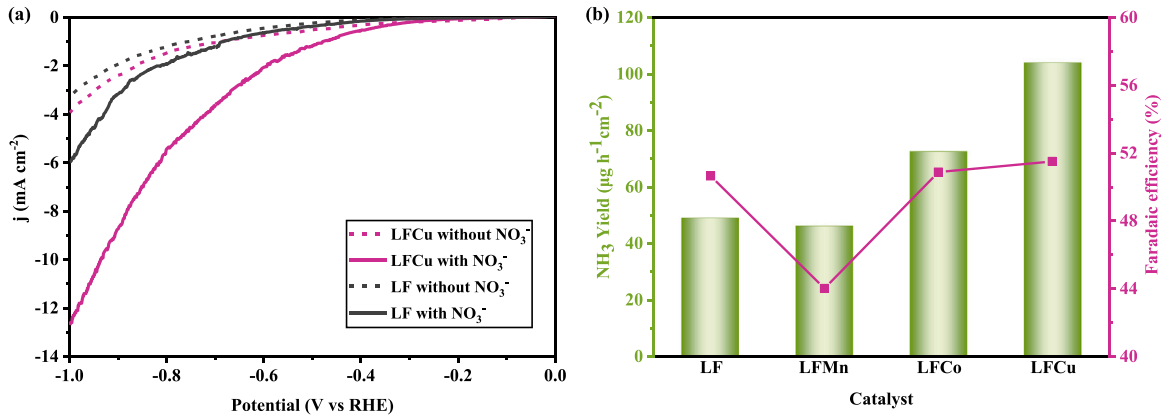

Fig. 5. (a) LSV curves of LF and LFCu in electrolyte with or without NO_3^-; (b) NH_3 yields and Faradaic efficiencies of LF, LFMn, LFCo, and LFCu at − 0.7 V (vs. RHE).

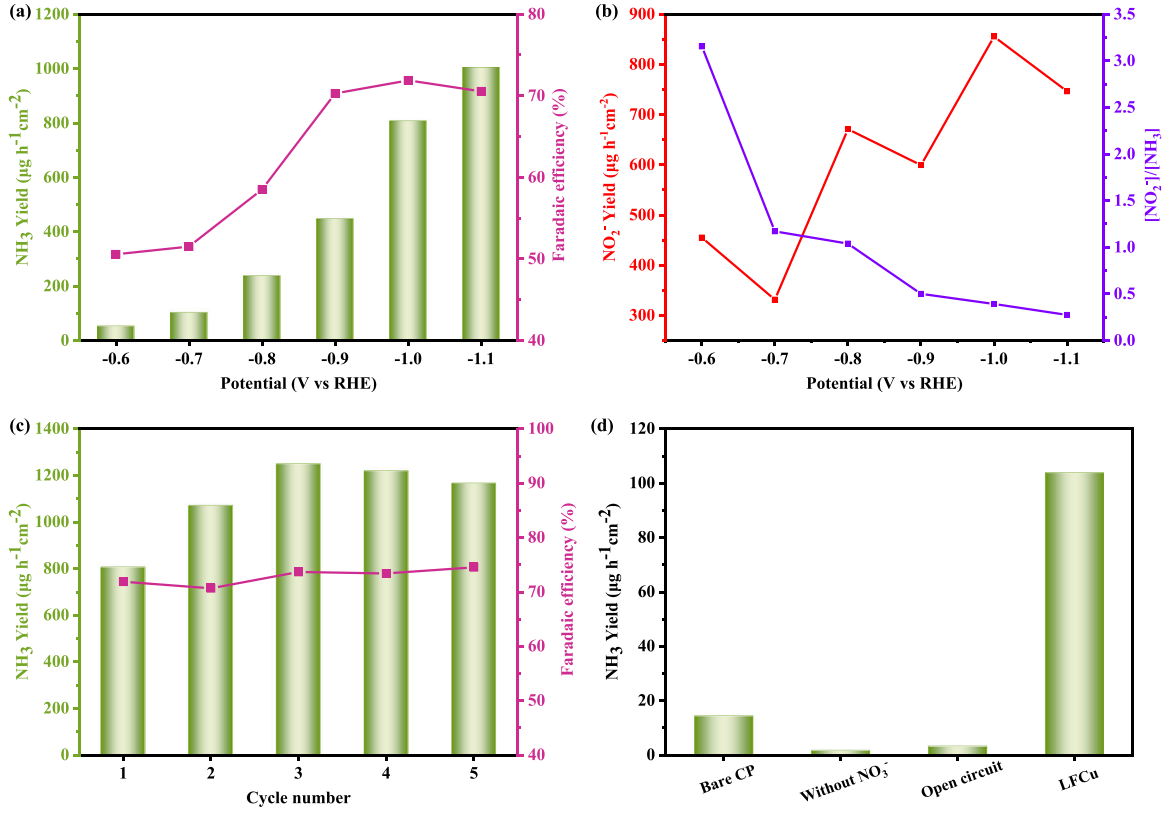

Fig. 6. (a) NH_3 yield and Faradaic efficiency of LFCu at different potentials; (b) NO_2^- yield and $[NO_2^-]/[NH_3]$ of LFCu at different potentials; (c) consecutive recycling experiments; (d) control experiments.

oxygen vacancies on the surface of LFCu. Thus the adsorption of NO_3^- was enhanced [22], and the N-O bonds were weakened and easy to break [20]. Therefore, the rate-determining step was enhanced, and the NH_3 yield was improved. In the selectivity-determining step, the intermediate, $*NO_2$, tended to bind to both oxygen vacancies [23] and Cu [8] rather than desorb to form the by-product, NO_2^-, thus the selectivity of NH_3 was enhanced. Besides, both oxygen vacancies and Cu^+/Cu^{2+} in LFCu could increase the interstitial states, improving the conductivity of the catalyst [7,22]. Based on the above reasons, LFCu performed well as an electrocatalyst to reduce NO_3^- to NH_3, and it may play a significant role in the industrialization of this technology.

4. Conclusions

In summary, we synthesized perovskite $LaFeO_3$ and transition metal (Mn, Co, Cu) doped $LaFeO_3$ by a sol-gel method. All the samples were subjected to various characterization tests and employed for electrochemical nitrate reduction to synthesize the desired product, ammonia. $LaFeO_3$ had a good electrocatalytic activity for the reduction of nitrate to ammonia. After doping with Co or Cu, oxygen vacancies were formed on the surface of the catalysts, which further enhanced the catalytic activity. The best catalyst among all the samples was Cu-doped $LaFeO_3$, which achieved the maximum ammonia yield of 1005.0 μg $h^{-1}cm^{-2}$ at − 1.1 V (vs. RHE) and the maximum Faradaic efficiency of 71.9% at − 1.0 V (vs. RHE). Moreover, the catalyst exhibited excellent stability in consecutive recycling experiments. The ammonia yield and the Faradaic efficiency increased rather than decreased during recycling. The ammonia yield was as high as 1250.5 μg $h^{-1}cm^{-2}$ in the third cycle, and the Faradaic efficiency was 74.5% in the fifth cycle at − 1.0 V (vs. RHE). This phenomenon could be attributed to the ferroelectricity of

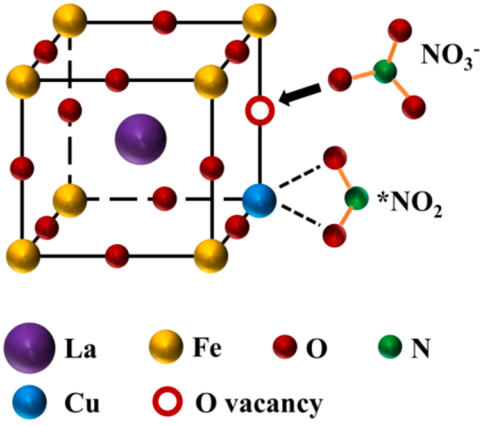

Fig. 7. Schematic model of electrocatalytic reduction of NO_3^- on LFCu.

lanthanum ferrite material. When the fresh catalyst underwent the first cycle, ferroelectric polarization occurred under the influence of the applied electric field. And then in the subsequent cycles, the residual polarization in the catalyst promoted the charge seperation and facilitated the charge transfer between the catalyst and the electrolyte. According to characterization tests and electrochemical experiments, we proposed the mechanism of the highly efficient electrochemical reduction of nitrate to ammonia on Cu-doped $LaFeO_3$. When a small amount of Fe^{3+} in the lattice of the catalyst was replaced by Cu^+/Cu^{2+}, oxygen vacancies were generated on the surface of the catalyst in order to achieve charge balance. The oxygen atoms in the nitrate would fill in the oxygen vacancies, which enhanced the adsorption of nitrate and weakened the N-O bond, thus promoting the conversion of nitrate to $*NO_2$. And the intermediate, $*NO_2$, tended to bind to oxygen vacancies and Cu rather than desorb to form nitrite, which improved the selectivity of ammonia in the products. Besides, both oxygen vacancies and Cu^+/Cu^{2+} in the catalyst could improve the conductivity of the catalyst. This work may broaden the avenue for the selection and modification of the catalysts for electrochemical ammonia synthesis in the future.

CRediT authorship contribution statement

Qi Yin: Conceptualization, Methodology, Validation, Formal analysis, Investigation, Data curation, Writing – original draft, Writing – review & editing. **Hao Zhou***: Conceptualization, Resources, Writing – review & editing, Supervision, Project administration, Funding acquisition.

Declaration of Competing Interest

The authors declare that they have no known competing financial interests or personal relationships that could have appeared to influence the work reported in this paper.

Acknowledgements

This work was supported by the Fundamental Research Funds for the Central Universities (2022ZFJH004).

Appendix A. Supporting information

Supplementary data associated with this article can be found in the online version at doi:10.1016/j.mtcomm.2023.106048.

References

[1] B. Suryanto, K. Matuszek, J. Choi, R.Y. Hodgetts, H.L. Du, J.M. Bakker, C. Kang, P. V. Cherepanov, A.N. Simonov, D.R. Macfarlane, Nitrogen reduction to ammonia at high efficiency and rates based on a phosphonium proton shuttle, Science 372 (6547) (2021) 1187–1191.
[2] Y. Wan, H. Zhou, M. Zheng, Z. Huang, F. Kang, J. Li, R. Lv, Oxidation state modulation of bismuth for efficient electrocatalytic nitrogen reduction to ammonia, Adv. Funct. Mater. (2021).
[3] X. Han, C.S. Gerke, S. Banerjee, M. Zubair, J. Jiang, N.M. Bedford, E.M. Miller, V. S. Thoi, Strategic design of MoO2 nanoparticles supported by carbon nanowires for enhanced electrocatalytic nitrogen reduction, ACS Energy Lett. 5 (10) (2020) 3237–3243.
[4] Z. Yan, M. Ji, J. Xia, H. Zhu, Recent advanced materials for electrochemical and photoelectrochemical synthesis of ammonia from dinitrogen: one step closer to a sustainable energy future, Adv. Energy Mater. 10 (11) (2019) 1902020.
[5] Y. Xu, M. Wang, K. Ren, T. Ren, M. Liu, Z. Wang, X. Li, L. Wang, H. Wang, Atomic defects in pothole-rich two-dimensional copper nanoplates triggering enhanced electrocatalytic selective nitrate-to-ammonia transformation, J. Mater. Chem. A 9 (30) (2021) 16411–16417.
[6] H. Wang, Q. Mao, T. Ren, T. Zhou, K. Deng, Z. Wang, X. Li, Y. Xu, L. Wang, Synergism of interfaces and defects: Cu/Oxygen vacancy-rich Cu-Mn3O4 heterostructured ultrathin nanosheet arrays for selective nitrate electroreduction to ammonia, ACS Appl. Mater. Interfaces 13 (37) (2021) 44733–44741.
[7] Wang H., Guo Y., Li C., Yu H., Deng K., Wang Z., Li X., Xu Y.& Wang L. , 2022. Cu/CuOx In-Plane Heterostructured Nanosheet Arrays with Rich Oxygen Vacancies Enhance Nitrate Electroreduction to Ammonia. ACS Applied Materials & Interfaces, 2022.
[8] G. Chen, Y. Yuan, H. Jiang, S. Ren, L. Ding, L. Ma, T. Wu, J. Lu, H. Wang, Electrochemical reduction of nitrate to ammonia via direct eight-electron transfer using a copper–molecular solid catalyst, Nat. Energy 5 (8) (2020) 605–613.
[9] X. Deng, Y. Yang, L. Wang, X.Z. Fu, J.L. Luo, Metallic Co nanoarray catalyzes selective NH3 production from electrochemical nitrate reduction at current densities exceeding 2 A cm−2, Adv. Sci. 8 (7) (2021) 2004523.
[10] Q. Hong, J. Zhou, Q. Zhai, Y. Jiang, M. Hu, X. Xiao, S. Li, Y. Chen, Cobalt phosphide nanorings towards efficient electrocatalytic nitrate reduction to ammonia, Chem. Commun. 57 (88) (2021) 11621–11624.
[11] Q. Yao, J. Chen, S. Xiao, Y. Zhang, X. Zhou, Selective Electrocatalytic Reduction of Nitrate to Ammonia with Nickel Phosphide, ACS Appl. Mater. Interfaces 13 (26) (2021) 30458–30467.
[12] P. Gao, Z.H. Xue, S.N. Zhang, D. Xu, G.Y. Zhai, Q.Y. Li, J.S. Chen, X.H. Li, Schottky barrier-induced surface electric field boosts universal reduction of NOx in water to ammonia, Angew. Chem. Int. Ed. 60 (38) (2021) 20711–20716.
[13] Z. Wu, M. Karamad, X. Yong, Q. Huang, D.A. Cullen, P. Zhu, C. Xia, Q. Xiao, M. Shakouri, F. Chen, J.Y. Kim, Y. Xia, K. Heck, Y. Hu, M.S. Wong, Q. Li, I. Gates, S. Siahrostami, H. Wang, Electrochemical ammonia synthesis via nitrate reduction on Fe single atom catalyst, Nat. Commun. 12 (2021) 1.
[14] Y. Wang, L. Zhang, Y. Niu, D. Fang, J. Wang, Q. Su, C. Wang, Boosting NH3 production from nitrate electroreductionvia electronic structure engineering of Fe3C nanoflakes, Green. Chem. 23 (19) (2021) 7594–7608.
[15] Q. Liu, Q. Liu, L. Xie, Y. Ji, T. Li, B. Zhang, N. Li, B. Tang, Y. Liu, S. Gao, Y. Luo, L. Yu, Q. Kong, X. Sun, High-Performance electrochemical nitrate reduction to ammonia under ambient conditions using a FeOOH nanorod catalyst, ACS Appl. Mater. Interfaces 14 (15) (2022) 17312–17318.
[16] J. Wang, D. Wu, M. Li, X. Wei, X. Yang, M. Shao, M. Gu, Bismuth ferrite as an electrocatalyst for the electrochemical nitrate reduction, Nano Lett. (2022).
[17] W. Yang, L. Yang, H. Peng, S. Lv, H. Muhammad Adeel Sharif, W. Sun, W. Li, C. Yang, H. Lin, Perovskite oxide LaMO3-δ (M = Fe, Co, Ni and Cu) cathode for efficient electroreduction of nitrate, Sep. Purif. Technol. 295 (2022), 121278.
[18] H. Zheng, Y. Zhang, Y. Wang, Z. Wu, F. Lai, G. Chao, N. Zhang, L. Zhang, T. Liu, Perovskites with enriched oxygen vacancies as a family of electrocatalysts for efficient nitrate reduction to ammonia, Small 19 (2023) 2205625.
[19] Y. Wang, H. Li, W. Zhou, X. Zhang, B. Zhang, Y. Yu, Structurally disordered RuO2 nanosheets with rich oxygen vacancies for enhanced nitrate electroreduction to ammonia, Angew. Chem. Int. Ed. 61 (2022) 19.
[20] R. Jia, Y. Wang, C. Wang, Y. Ling, Y. Yu, B. Zhang, Boosting selective nitrate electroreduction to ammonium by constructing oxygen vacancies in TiO2, ACS Catal. 10 (6) (2020) 3533–3540.
[21] B. Cao, X. Xu, Z. Hong, J. Liao, P. Li, H. Zhang, S. Duo, Oxygen-vacancy-containing Nb2O5 nanorods with modified semiconductor character for boosting selective nitrate-to-ammonia electroreduction, Sustain. Energy Fuels 6 (8) (2022) 2062–2066.
[22] X. Zhang, C. Wang, Y. Guo, B. Zhang, Y. Wang, Y. Yu, Cu clusters/TiO2−x with abundant oxygen vacancies for enhanced electrocatalytic nitrate reduction to ammonia, J. Mater. Chem. A 10 (12) (2022) 6448–6453.
[23] Y. Wang, S. Shu, M. Peng, L. Hu, X. Lv, Y. Shen, H. Gong, G. Jiang, Dual-site electrocatalytic nitrate reduction to ammonia on oxygen vacancy-enriched and Pd-decorated MnO2 nanosheets, Nanoscale 13 (41) (2021) 17504–17511.
[24] Q. Peng, B. Shan, Y. Wen, R. Chen, Enhanced charge transport of LaFeO3 via transition metal (Mn, Co, Cu) doping for visible light photoelectrochemical water oxidation, Int. J. Hydrog. Energy 40 (45) (2015) 15423–15431.
[25] K. Chu, F. Liu, J. Zhu, H. Fu, H. Zhu, Y. Zhu, Y. Zhang, F. Lai, T. Liu, A general strategy to boost electrocatalytic nitrogen reduction on perovskite oxides via the oxygen vacancies derived from A-Site deficiency, Adv. Energy Mater. 11 (11) (2021) 2003799.
[26] X. Hu, Y. Sun, S. Guo, J. Sun, Y. Fu, S. Chen, S. Zhang, J. Zhu, Identifying electrocatalytic activity and mechanism of Ce1/3NbO3 perovskite for nitrogen reduction to ammonia at ambient conditions, Appl. Catal. B: Environ. 280 (2021), 119419.

[27] Z. Wang, J. Shen, W. Fu, J. Liao, J. Dong, P. Zhuang, Z. Cao, Z. Ye, J. Shi, M. Ye, Controlled oxygen vacancy engineering on In2O3−x/CeO2−y nanotubes for highly selective and efficient electrocatalytic nitrogen reduction, Inorg. Chem. Front. (2020).
[28] J. Jeong, C. Song, K. Kim, W. Sigmund, J. Yoon, Effect of Mn doping on particulate size and magnetic properties of LaFeO3 nanofiber synthesized by electrospinning, J. Alloy. Compd. 749 (2018) 599–604.
[29] Y. Ji, Y. Xie, L. Zheng, F. Xu, Efficient activation of peroxymonosulfate by porous Co-doped LaFeO3 for organic pollutants degradation in water, J. Solid State Chem. 297 (2021), 122077.
[30] G. Wang, C. Cheng, J. Zhu, L. Wang, S. Gao, X. Xia, Enhanced degradation of atrazine by nanoscale LaFe1-xCuxO3-δ perovskite activated peroxymonosulfate: performance and mechanism, Sci. Total Environ. 673 (2019) 565–575.
[31] X. Fan, C. Ma, D. Zhao, Z. Deng, L. Zhang, Y. Wang, Y. Luo, D. Zheng, T. Li, J. Zhang, S. Sun, Q. Lu, X. Sun, Unveiling selective nitrate reduction to ammonia with Co3O4 nanosheets/TiO2 nanobelt heterostructure catalyst, J. Colloid Interface Sci. 630 (2023) 714–720.
[32] J. Li, D. Zhao, L. Zhang, Y. Ren, L. Yue, Z. Li, S. Sun, Y. Luo, Q. Chen, T. Li, K. Dong, Q. Liu, Q. Kong, X. Sun, Boosting electrochemical nitrate-to-ammonia conversion by self-supported MnCo2O4 nanowire array, J. Colloid Interface Sci. 629 (2023) 805–812.
[33] J. Gao, B. Jiang, C. Ni, Y. Qi, X. Bi, Enhanced reduction of nitrate by noble metal-free electrocatalysis on P doped three-dimensional Co3O4 cathode: mechanism exploration from both experimental and DFT studies, Chem. Eng. J. 382 (2020), 123034.
[34] Y. Zhu, W. Zhou, J. Yu, Y. Chen, M. Liu, Z. Shao, Enhancing electrocatalytic activity of perovskite oxides by tuning cation deficiency for oxygen reduction and evolution reactions, Chem. Mater. 28 (6) (2016) 1691–1697.
[35] Y. Cong, Z. Geng, Y. Sun, L. Yuan, X. Wang, X. Zhang, L. Wang, W. Zhang, K. Huang, S. Feng, Cation segregation of A-Site deficiency perovskite La0.85FeO3−δNanoparticles toward high-performance cathode catalysts for rechargeable Li-O2 battery, ACS Appl. Mater. Interfaces 10 (30) (2018) 25465–25472.
[36] H.S. Kushwaha, A. Halder, R. Vaish, Ferroelectric electrocatalysts: a new class of materials for oxygen evolution reaction with synergistic effect of ferroelectric polarization, J. Mater. Sci. 53 (2) (2018) 1414–1423.
[37] A. Kakekhani, S. Ismail-Beigi, E.I. Altman, Ferroelectrics: a pathway to switchable surface chemistry and catalysis, Surf. Sci. 650 (2016) 302–316.
[38] S. Gao, H. Ji, P. Yang, M. Guo, J. Tressel, S. Chen, Q. Wang, High-Performance photocatalytic reduction of nitrogen to ammonia driven by oxygen vacancy and ferroelectric polarization field of SrBi4Ti4O15 nanosheets, Small 19 (2023) 2206114.